



Effects of Foil Thickness to Grain Size (t/d) Ratio and Prestraining on Tensile Response, Microformability and Crystallographic Texture of Ultra-Low Carbon Steel Thin Foils

Javed S. Ibrahim¹ · M. J. N. V. Prasad¹ · Partha Sarkar² · K. Narasimhan¹

Received: 3 June 2023 / Accepted: 4 August 2023 / Published online: 4 September 2023
© The Author(s) under exclusive licence to The Korean Institute of Metals and Materials 2023

Abstract

Ultra-low carbon (ULC) steels, containing a carbon content ~ 0.055 wt%, have been used in several applications in the form of thin foils. However, there are limited studies on the effects of foil thickness (t) to grain size (d) ratio and foil condition on the tensile response and formability of thin ULC steel foils. In the present work, the tensile and forming behaviours of ULC steel foils of thickness about 400 μm were evaluated in both annealed and prestrained (by cold reduction to 2–7%) conditions as a function of t/d ratio and followed by detailed texture evolution analysis. Vacuum annealing was used to achieve varying t/d ratios in the specimens. Additionally, thin ULC steel foils of 100 μm thickness in annealed condition were also used for examining the thickness effect. Microstructural analysis was performed using the electron backscattered diffraction technique. Microformability was assessed by a miniaturised Nakazima test setup with specimen geometries designed to produce three different strain paths. The annealed foils displayed a typical yield-point phenomenon, but the total yield-point elongation decreased with decreasing thickness and grain size. The foils exhibited typical Hall–Petch strengthening, cold work hardening, and forming limit curves; however, there were substantial reductions in both tensile strength and ductility, and consequently, the forming strains, with decreasing the t/d ratio. The tensile response and formability of the foils were adversely affected by both thinning and prestraining. The texture studies revealed the formation of a γ -fibre i.e., $\langle 111 \rangle$ normal direction, and its intensity varied significantly with the t/d ratio and mode of strain path.

Keywords Low carbon steel · Thin foils · Tensile properties · Forming limit curves · Texture

1 Introduction

Low-carbon steels ($< 0.25\%$ C) are highly sought-after in applications pertaining to automobile body components, structural shapes, pipes, construction bridge components, and food cans. The superior ductility (which is a prerequisite for better formability) of low-carbon steels has accorded them an edge over their higher-carbon counterparts in sheet-forming applications. The superior ductility stems from the decreased presence of interstitial, which has a detrimental

effect on the formation of the γ -fibre $111 \rangle$ normal direction component, leading to a lower value of the Lankford coefficient and thereby poor formability. The presence of low carbon content compensates for the reduction of γ -fibre $\langle 111 \rangle$ normal direction (during recrystallization) by increasing the $(111) [112]$ component of γ -fibre during the later stages of recrystallization [1]. The industry-prescribed criteria for desirable “ r ” values for deep drawing operations within the range of 1.6 to 2.0 are met by low-carbon steels such as ultra-low carbon and interstitial-free (IF) steels [2]. Process parameters such as hot rolling conditions, annealing temperature, and skin-pass parameters have a profound influence on the formability of low-carbon steels [3, 4]. As a result, there exists a strong quest among the metallurgists for the conceptualization of the processing parameters–mechanical behaviour correlation of low-carbon steels [5].

A well-known characteristic of low-carbon steels is the yield-point phenomenon [6]. The occurrence of this phenomenon is related to the interaction of interstitial carbon

✉ Javed S. Ibrahim
javedsibrahim@gmail.com

¹ Department of Metallurgical Engineering and Materials Science, Indian Institute of Technology Bombay, Mumbai 400 076, India

² Theis Precision Steel India Private Limited, Navsari, Gujarat 396 424, India

atoms with dislocations after the start of initial yielding. The localised yielding spreads uniformly throughout the stressed regions, causing the formation of Luders bands. Strain hardening begins after the Luders bands spread entirely through the deformation zone. During stamping operations on steel sheets, the Luders bands are undesirable. The failure of the Luders bands to traverse across the entire sheet leads to an undesirable surface roughness, known as stretcher strain lines. In industrial practise, the elimination of the aforementioned problem is attained by subjecting the annealed sheets to a mild deformation by bending or low percent cold rolling reduction (skin-pass rolling). Also, it is unnecessary to deform the entire cross-section of the sheet to eliminate the yield point effect. Proper dispersion of deformed regions is required to prevent any localised thinning during the forming process [7].

The yield-point phenomenon and its detrimental effect on sheet-forming operations have led to the exploration and analysis of various strategies to combat the issue. An early study investigated the effects of different levels of prestraining ($\epsilon \sim 0.05\text{--}0.20$) on the tensile yield stress value alongside the consideration of the anisotropy of the low-carbon steel sheet by preparing tensile specimens at different angles with the rolling direction (RD). The same study also encompassed a simulative approach to acquire an idea of the development of deformation textures and intragranular microstructures. The conclusion revealed a 20% increase in yield strength for a prestrain of 0.15 [3]. In order to understand the relation between the extent of skin-pass, the strain hardening exponent, and the mean ' \bar{r} ' value, it was asserted via measured data that dislocation density is very sensitive to prestrain (skin-pass). Since any change in dislocation density can considerably influence the strain hardening exponent, skin pass reduction should not be performed at the expense of a change in strain hardening coefficient, which is possible through careful optimisation of the reduction percentage.

There has been an increased demand for downgauging various metallic components with the intention of making compact devices/parts. This can lead to a well-known phenomenon termed the 'size effect'. The size effect in polycrystalline materials can be either intrinsic or extrinsic. The grain size of a material is one of the intrinsic factors, whereas the specimen size comes under the category of an extrinsic factor. The ratio between the specimen thickness (t) and the grain size (d) considers both types of factors for a polycrystalline material and has paramount importance, especially when the component size becomes smaller. There have been quite a number of studies on understanding the effect of t/d ratio on the mechanical behaviour of metallic materials, especially Cu, Ni, and Al-based face-centred cubic (FCC) metallic materials [8–10]. These studies have found a decrease in flow stress with decreasing specimen thickness at t/d ratios below a critical value, and a marked change in

percent elongation and mode of fracture was evident at very low t/d ratios. At lower length scales, size-dependent behaviour is prominent as a result of the individual properties of grains influencing the overall material behaviour to a huge extent. Furthermore, studies have revealed that the t/d ratio influences the micro-formability of thin foils [11].

It is worth mentioning that ULC steels, a category of low carbon steels, find numerous applications in switchboard components, Ni–Cd battery components, stamped shims in the automobile industry, etc., in the form of thin foils. The pronounced prevalence of size effects in thin foils due to the presence of few grains across thickness makes the t/d ratio a crucial aspect in the study of the deformation behaviour of steel (body-centred cubic structure) foils as well. There is very scant literature covering aspects pertaining to the effects of t/d ratio, material condition, and strain path variation (or) forming behaviour of thin steel foils with thickness less than 500 μm [12, 13]. The outcomes of these studies showcase a significant influence of the t/d ratio on the forming behaviour of foils with low thickness, changes in Hall–Petch behaviour with different levels of prestraining, etc. Moreover, a study of the interactive effect of all the above-mentioned factors on deformation behaviour of BCC metals and alloys has hardly been carried out in the past.

In view of the above-mentioned gaps in the literature, the present study is aimed at evaluating the tensile response as well as the formability of ULC steels (BCC alloy) in both annealed and prestrained conditions as a function of the t/d ratio. In addition, texture evolution under the combined effects of the t/d ratio, the state of the material, and the strain path are also investigated. This is primarily due to the tendency of thin foils to show a stark difference in mechanical behaviour from that of the widely studied bulk polycrystalline steel sheets.

2 Materials and Experimental Methods

2.1 Materials

Extra deep drawn (EDD) quality grade CR4 ULC steel foils containing $\sim 0.055\%$ C supplied by Theis Precision Steel Ltd., Gujarat, India were used for the present study. The steel foils are of thicknesses of 400 μm and 100 μm . The as-received 400 μm thick ULC steel foils were batch annealed followed by industrial skin-pass to a strain of $\sim 2\%$. These as-received foils were subsequently annealed under vacuum in a laboratory in order to obtain foils with three different t/d ratios. Further, the selected annealed foils were prestrained to just 7% cold reduction by a laboratory rolling mill of Buhler™ make, which led to a slight reduction in the foil thickness to $\sim 370 \mu\text{m}$. The as-received 100 μm foils were already in annealed condition.

2.2 Uniaxial Tensile Testing and Microforming Test

Typical dog-bone Extra deep drawn (EDD) quality grade CR4 ULC steel foils containing 0.055% C supplied by Theis Precision Steel Ltd., Gujarat, India, were used for the present study. The steel foils are of thicknesses of 400 μm and 100 μm . The as-received 400 μm thick ULC steel foils were batch annealed followed by industrial skin-pass to a strain of 2%. These as-received foils were subsequently annealed under vacuum in a laboratory in order to obtain foils with three different t/d ratios. Further, the selected annealed foils were prestrained to just 7% cold reduction by a laboratory rolling mill of BuhlerTM make, which led to a slight reduction in the foil thickness to 370 μm . The as-received 100- μm foils were already in annealed condition.

2.3 Uniaxial Tensile Testing and Microforming Test

Typical dog-bone tensile specimens were prepared in miniaturised dimensions of 5 mm gauge length and 2 mm gauge width (shown in Fig. 1a) by following the ASTM E8 standard and were machined by wire-cut electric discharge machining (EDM) followed by fine polishing to reduce the surface roughness. The uniaxial tensile testing was performed until failure at room temperature under an initial strain rate of $1 \times 10^{-3} \text{ s}^{-1}$ using an INSTRON 3345 tabletop universal testing machine (UTM) comprising a 5 kN load cell and proper customised mechanical grips. Sub-sized specimen geometries complying with the conventional Nakazima punch test [14] were prepared from both annealed and prestrained ULC foils and tested using a miniaturised and customised setup consisting of a hemispherical punch having a 15 mm diameter, a suitable blank holder, and tightening clamps. The microforming experiment was carried out using the same INSTRON 3345 UTM. Three distinct specimen geometries were used to study deformation along uniaxial, plane strain, and biaxial strain paths in the specimens to assess the formability of ULC steel foils. The specimens whose dimensions are shown in Fig. 1b were machined using wire-cut EDM and then mechanically polished using fine-grit SiC abrasive paper. A pattern with 1 mm-diameter dots with an equal spacing of 0.5 mm, as shown in Fig. 1c, was screen-printed on the forming test specimens. A forming speed of 0.015 ms⁻¹ was employed to deform the specimens until fracture. The corresponding changes in the dot dimensions in the vicinity of crack post-deformation were measured using an Olympus DSX100 opto-digital microscope for the major and minor strain values calculations. It is to be noted that these strain values for each corresponding strain path were considered the limiting strains for constructing the limit curves.

2.4 Microstructure and Crystallographic Texture Characterization

The microstructural examination of the ULC steel foils was performed using an FEI Quanta 3D scanning electron microscope (SEM) attached to an EDAX- electron backscattered diffraction (EBSD) detector. The EBSD scans were performed with the electron beam perpendicular to the rolling direction of ULC steel foils. In addition, the EBSD scans were obtained on selected microformed specimens (i.e., uniaxially and biaxially stretched specimens). The electron beam was incident on the outer surface of the hemispherical dome shape (proximal to the fractured area) produced in the foils. The samples for EBSD measurements were initially polished mechanically by using 600, 1500 and 2500 grit abrasive papers, followed by diamond polishing by applying 0.25 μm diamond paste on a velvet cloth of good quality, cut to a circular shape and mounted on a rotating polishing wheel that was run at slower speeds < 100 rpm for 45 min to ensure good surface finish. The samples were electropolished in a fully automatic, microprocessor controlled Struers Lectropol-5 electrolytic polishing apparatus in an electrolytic solution made of 80% methanol and 20% perchloric acid at 14 V output voltage for a duration of ~ 20 s. The temperature of the solution was maintained at 0 °C. In the deformed dome shaped samples, the domes were carefully cut from the rest of the specimens, and the area of the domes near to the fractured portions were polished in the similar fashion as mentioned earlier except that the mechanical polishing was done with finer grit sizes > 2000 in a very gentle manner. The scans were then performed on those polished portions. The EBSD scans covering more than 500 grains for each condition with a step size of 0.3 μm were obtained in order to ensure statistical reliability for better texture analysis. The TSL-OIM v8 software was used to analyse the raw EBSD data. A minimum confidence index (CI) of 0.1 was set for standard cleanup processing of the EBSD raw data. The grain size was established by considering the value of the average grain diameter measured by the equivalent circular diameter method. Bulk X-ray texture measurements were also performed to analyse the volumetric texture of selected samples before and after forming. These measurements were obtained using a solid-state Pixel-Quad detector in a Panalytical-Empyrean goniometer system having a power rating of 30 kW with a Cu-K α X-ray source. The bulk X-ray results were presented in the form of orientation distribution functions (ODF) after post-processing the raw data using Matlab software.

3 Results

3.1 Initial Microstructures

Figures 2 and 3 present coloured inverse pole figures (IPF) showcasing the microstructures of ULC steel foils in annealed and prestrained conditions taken on the surface of the foils. Figure 2a–c are of 400 μm thick foils with three different average grain sizes of $33 \pm 3 \mu\text{m}$, $60 \pm 5 \mu\text{m}$ and $100 \pm 11 \mu\text{m}$. These samples represent the t/d ratios of 12, 7 and 4, respectively. While Fig. 2d presents the microstructure of thin foil 100 μm thick with an average grain size of $35 \pm 4 \mu\text{m}$, which is nearly identical to that of the fine grain size of the annealed 400 μm thick sample. However, it is to be noted that its t/d ratio of ~ 3 is near that of the coarsest grain structure of a 400 μm thick sample. Figure 3a shows the microstructure of industry prestrained sample, whereas Figs. 3b and c present the microstructures of 7% prestrained samples with nearly the same thickness of 400 μm but having two different average grain sizes, respectively. The microstructures of the samples shown in Figs. 2a, 3a, and b represent the effect of prestrain level (0, 2 and 7%), as they contain almost similar grain sizes. The grain structures of all the samples are nearly equiaxed. Bulk X-ray texture (macrotexture) measurement results of all the starting samples are shown later in Figs. 8 and 9 for assessing the effect of deformation on texture evolution. Nevertheless, both microtexture and macrotexture results indicated the predominant presence of $\langle 111 \rangle$ ND γ -fiber in all the samples. As mentioned in the previous section, the starting sample used for annealing and further prestraining was batch annealed plus skin-passed foil. This sample has shown typical γ -fiber favourable for higher values [1]. The annealed samples showed double fibre texture, i.e., strong γ -fiber along with the development of slight θ -fiber i.e., $\langle 001 \rangle$ ND component. It is noted that there were no noticeable changes in the microstructure and texture of the samples upon further prestraining to 7%.

3.2 Uniaxial Tensile Response

Figures 4a and b show the tensile stress–strain curves of the annealed and prestrained foils, respectively. The properties include the yield strength, the tensile strength, the total elongation to failure, and uniform and non-uniform (post-necking) strains of both the types of foils are listed in Table 1. All the annealed foils exhibited the typical yield-point phenomenon i.e., upper and lower yield points (yield drop) followed by slight serrations at lower yield point with yield-point elongation in the range of 2–5%. The tensile specimens displayed Luders band formation and propagation during yielding. The total yield-point elongation decreased relatively with decreasing both the grain size

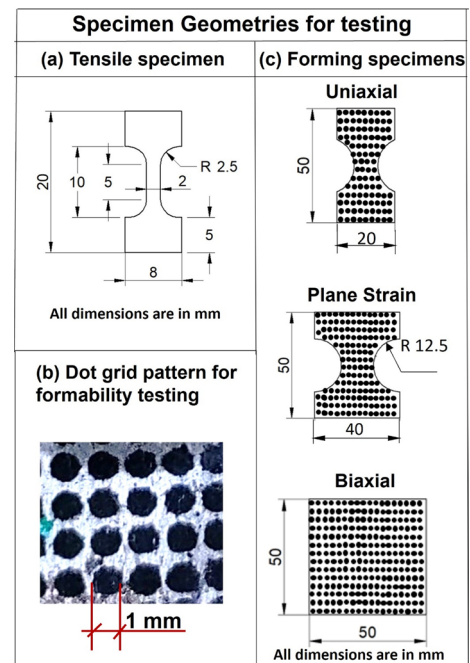


Fig. 1 Geometry of specimens used for **a** uniaxial tensile testing and **b** microforming test, and **c** the typical printed dot grid pattern on microforming specimens used for the strain measurement

and thickness of foil. This could be related to the reduced characteristic length scale for Luders band, slip and dislocations movement. The annealed ULC foils having fixed thickness (400 μm) exhibited increase in both the yield and tensile strengths with a decrease in the grain size. The total elongation to failure was reduced from $\sim 48\%$ to 38% in the thick and coarse-grained foil representing $t/d \sim 4$. It could be observed that the 100 μm thick foil ($d \sim 35 \mu\text{m}$) exhibited lower strength and ductility with a lesser prevalence of Luders bands than its thicker counterpart with similar grain size. This highlights the fact that ductility can be reduced with reduction in thickness, and the difference in the yield-point values may be due to the variation in pre-processing causing dissimilar Luders bands.

In Fig. 4b, as anticipated, the yield-drop behaviour was observed to be clearly eliminated in all the prestrained samples. The industrially prestrained foil (subjected to $\sim 2\%$ reduction) showed similar ductility as that of the annealed foils and the reason being the lower amount of prestraining. In addition to the considerable increase in yield and tensile strengths in the laboratory prestrained samples, a significant reduction in ductility and negligible strain hardening ability was observed in the samples with t/d ratio ~ 7 , whereas the reduction in ductility and strain hardening ability of the sample with t/d ratio ~ 12 was comparatively lower. The laboratory prestrained samples, which underwent 7% reduction in thickness showed reduced uniform strain than their industry prestrained

counterpart. These aspects are addressed in discussion section.

3.3 Microformability

3.3.1 Forming Limiting Curves

Microformability was evaluated for annealed and prestrained ULC steel samples by deforming the foils of different t/d ratios in uniaxial, plane strain, and biaxial strain paths using the miniature Nakazima setup. The forming limit diagrams (FLD) for the annealed and prestrained ULC steel foils are shown in Figs. 5a and b, respectively. A few basic observations could be made upon analysing the forming limiting curve (FLC) of the samples in different conditions as a function of the t/d ratio:

1. Most of the samples displayed typical FLCs. However, except for the annealed foil with $t/d \sim 12$, all other foils exhibited either equal or lower formability under biaxial stretching than that in the plane strain path.
2. The prestrained foils exhibited lower forming limit strains than the annealed foils for the same t/d ratio, which is relatable to the tensile ductility.
3. Among the annealed foils studied, for similar grain sizes, the foil thickness proved to be important, as the thinner foil showed a very low forming limit.
4. In the case of annealed foils of the same thickness, the limiting strains decreased with increasing grain size or decreasing the t/d .
5. The in-plane uniaxial tensile elongation and out-of-plane uniaxial stretching elongation (major strain value) were comparable to an extent in most cases.

3.3.2 Evolution of Microstructure and Texture under Uniaxial and Biaxial Strain Paths

Figures 6 and 7 show the IPF maps obtained from EBSD data illustrating the evolution of microstructure in the annealed and prestrained samples, respectively, subjected to uniaxial and biaxial stretching strain path modes. There was significant elongation of the grains near the fracture region, but the direction and total stretching of the grain

Fig. 2 Coloured inverse pole figure (IPF) maps of 400 μm thick annealed ULC steel foils with different average grain sizes of **a** 33 μm , **b** 60 μm and **c** 100 μm , and **d** of 100 μm thick annealed ULC steel foil with an average grain size of 35 μm

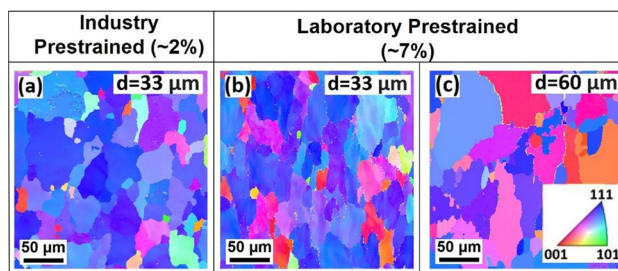
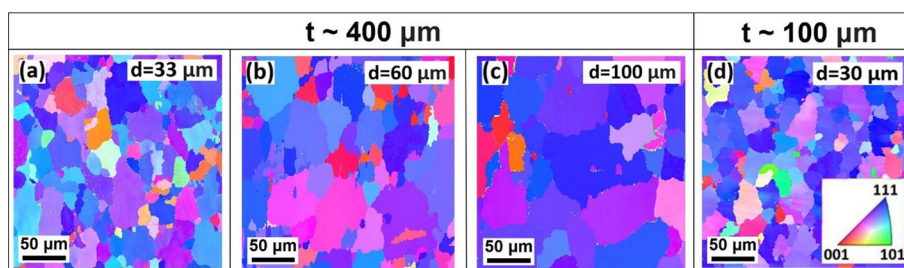


Fig. 3 Coloured inverse pole figure (IPF) maps of $\sim 40 \mu\text{m}$ thick **a** industry prestrained foil with an average grain size of 33 μm , and of laboratory prestrained foils with two different average grain sizes of **b** 33 μm and **c** 60 μm

structure varied with the strain path and the amount of effective strain experienced by each sample. Since the total number of grains captured by EBSD near the fracture region was limited, the microtexture information from EBSD-IPF maps is not adequate to assess the texture evolution in the thin foils. Hence, bulk X-ray texture measurements were performed on the samples before and after forming under two different strain paths. Figures 8 and 9 present the orientation distribution functions (ODF) in terms of $\varphi_2 = 45^\circ$ sections obtained by analysing the bulk X-ray data for the annealed and prestrained samples in both undeformed and two different strain paths i.e., uniaxial and biaxial stretching conditions. It is noted that the initial γ -fiber texture present in both annealed and prestrained samples strengthened further, especially the $\{111\} \langle 110 \rangle$ components lying in the fiber direction during forming. These were intensified more under biaxial stretching than in uniaxial strain path (Figs. 8 e, i and 9 d, g). Similarly, the $\{001\} \langle 110 \rangle$ components present in the θ -fiber texture in the annealed samples got strengthened slightly under deformation. Furthermore, the changes in texture were substantial in the samples that experienced larger effective strain, for example, the fine-grained ($d \sim 33 \mu\text{m}$) 400 μm thick foils in both annealed and prestrained conditions.

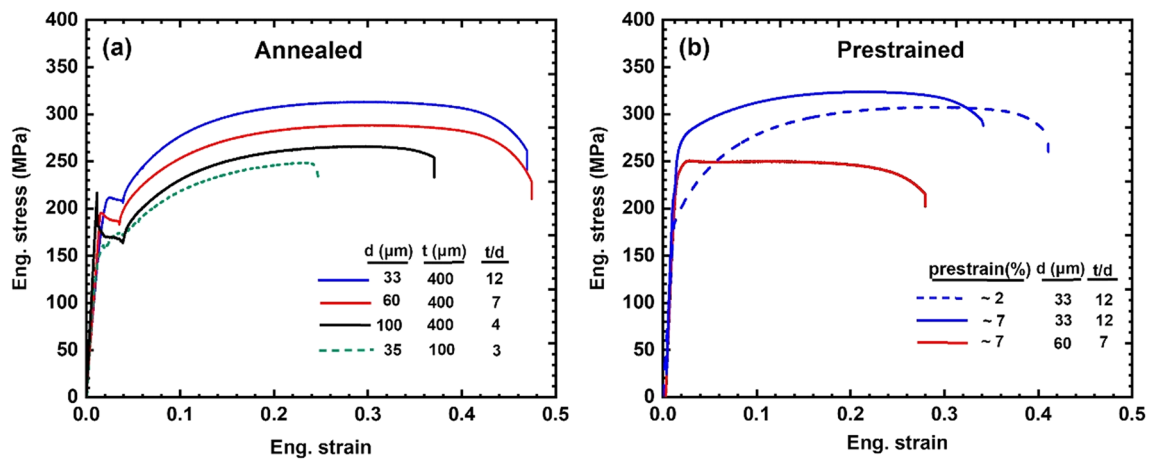


Fig. 4 Engineering tensile stress–strain curves of **a** annealed foils and **b** Prestrained foils with different t/d ratios obtained at room temperature under an initial strain rate of $1 \times 10^{-3} \text{ s}^{-1}$

4 Discussion

4.1 Tensile Behaviour of ULC steels

The ULC steel samples showed the yield-point phenomenon, which is expected, in the annealed condition (Fig. 4a). Importantly, there was a moderate increase in the extent of the yield drop phenomenon with the lowering of t/d ratios. That means the different annealing regimes did not cause a significant change in the Luders bands. The decrease in strength with decreasing t/d ratio is a result of increasing the grain size (low t/d ratio samples are coarse-grained foils) leading to lesser grain boundary obstruction to dislocation motion, which is a well-established phenomenon. In the case of prestrained foils (Fig. 4b), the negligible difference in ductility and yield point in the industrially prestrained foil (subjected to ~2% reduction) compared to the annealed foil of t/d ratio ~12, is mostly due to the lower amount of prestraining. In the

7% prestrained samples, there was a noticeable increase in the yield strength values for the two t/d ratios of 12 and 6. The prestraining/skinpass is commonly known to produce a drop in the yield stress value; however, cold reduction percentage exceeding 4% i.e., beyond yield-point elongation can result in increase in the yield strength [15]. This could be due to the fact that prestraining process, which is actually intended to relieve the pinned dislocations from the solute carbon atoms causing a drop in yield stress, when performed at higher reduction percentages (>4%) increases the yield stress as result of work hardening. The prestrained specimen with $t/d \sim 7$ showed significant reduction in total elongation to failure compared to the specimen with $t/d \sim 12$, though such change was not observed in the counterpart annealed specimens. This trend can be addressed through the following hypothesis. The prestraining process induces Luders bands (localized yielding regions) at localized portions mainly in the surface of the foil and very unlikely in the sheet interior. These localized yielding regions span no more than 2–3 grains across the sheet thickness. The surface of a prestressed specimen

Table 1 Tensile properties of the annealed and prestrained ULC steel foils (updated)

Material condition	Foil thickness, t (μm)	Grain size, d (μm)	t/d	Yield strength, σ_y (MPa)	Tensile strength, σ_T (MPa)	Total elongation (%)	Uniform strain, ϵ_u (%)	Non-uniform strain, ϵ_{nu} (%)
Annealed	400	33 ± 3	12	204, 186	310, 295	47, 42	32, 29	15, 13
	400	60 ± 5	7	183, 163	285, 270	48, 41	31, 28	17, 13
	400	100 ± 11	4	160, 134	261, 239	37, 30	30, 23	8, 7
	100	35 ± 4	3	163, 135	245, 218	22, 17	20, 14	2, 3
2% Prestrained	400	33 ± 3	12	197, 178	304, 288	42, 39	33, 28	9, 11
7% Prestrained	400	33 ± 3	12	248, 229	316, 302	33, 27	21, 19	12, 8
7% Prestrained	400	60 ± 4	7	232, 210	242, 227	27, 21	2, 1.5	25, 19.5

encompasses deformed grains combined with undeformed ones. When the prestrained specimens were subsequently subjected to minimal uniaxial tensile strains, the extent of localized yielding regions in the surface remains the same. Further deformation facilitates the proliferation of the localized yielding regions into undeformed areas in the centre of the sheet/foil till the failure of the material [16]. Therefore, the lower ductility of the prestrained specimen with $t/d \sim 7$ could be attributed to the presence of localized yielding regions in the two layers of grains close to the surface of the foil which forms a majority (due to lower t/d ratio) in these specimens, accounting for their earlier start of yielding and consequently premature failure compared to specimens with higher t/d ratio. It can be stated that the behaviour of the 7% prestrained samples relies on three important factors such as the initial grain size of the samples, the extent of discontinuous yielding (Luders bands) and the higher dislocation density induced by the prestraining process.

Similarly, the thin sample ($t \sim 100 \mu\text{m}$) with lower $t/d \sim 3$ displayed reduced total elongation to failure as compared to the counterpart thick annealed sample with $t/d \sim 12$. This kind of behaviour was observed in the electrodeposited copper [17] and reported in commercial copper as well [8, 9]. This has been explained in terms of contribution of the increased surface grains fraction in thin foils for a given grain size leading to premature failure. In addition, there was significant reduction in both upper and lower yield-point stresses in the thin ULC steel foil ($t/d \sim 3$) as compared to that in the thick foil ($t/d \sim 12$). However, the effect of specimen thickness on decrease in the yield strength is quite unusual in FCC materials. It is suspected to be related to the yield-point phenomenon observed in the ULC steel. As per as Cottrell theory [18], the interstitial atoms such as carbon and nitrogen interact with the moving dislocations in steels involving pinning and unpinning action (Cottrell

atmosphere) during application of external stress leading to serrations during yield-point elongation and results in solute hardening as well. According to Johnston and Gilman theory [19], there two important criteria for the yield drop: (i) the number of moving dislocations should increase, and (ii) there should be a direct relationship between the stress and the velocity of the dislocations. As compared to FCC metals, BCC metals like iron, by virtue, contain a relatively lesser number of mobile dislocations due to a higher number of slip systems. Moreover, the mobile dislocation is expected to decrease further in the thinner foils due to the increased surface grain fraction (broken bond atoms) leading to reduced solute-dislocation interaction and thereby, decreased yield stress for a given grain size of low carbon steels.

4.2 Hall–Petch Relationship

Hall–Petch relationship is the widely acclaimed relation between yield strength (σ_y) and grain size(d) of polycrystalline materials [20, 21]. It is given by

$$\sigma_y = \sigma_0 + k_{HP}d^{-1/2}$$

where σ_0 is the friction stress and k_{HP} is the Hall–Petch coefficient. The term σ_0 signifies the requirement of stress to move individual dislocations inside a grain, whereas k_{HP} indicates the requirement of local intensified stress for initiating and triggering general yielding across grain boundaries. Figure 8a (updated) shows the σ_y versus $d^{-1/2}$ (a typical Hall–Petch) plot for the data of both annealed and prestrained ULC foils. The material constants σ_0 and k_{HP} were computed by fitting the data with a linear relationship between σ_y and $d^{-1/2}$. It was determined that $\sigma_0 \sim 110 \text{ MPa}$ and $k_{HP} \sim 592 \text{ MPa } \mu\text{m}^{-1/2}$ for the annealed foils, whereas for prestrained (7% reduction) foils, $\sigma_0 \sim 167 \text{ MPa}$ and

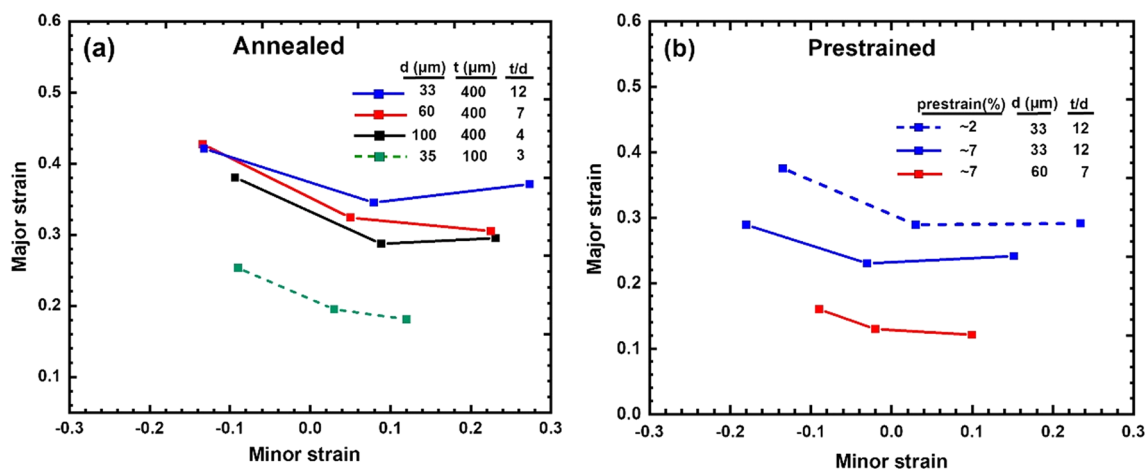


Fig. 5 Forming limit curves of **a** annealed foils and **b** prestrained foils with different t/d ratios

Fig. 6 Coloured inverse pole figure (IPF) maps of four different annealed samples after microforming under **a–d** uniaxial stretching and **e–h** biaxial stretching. Here, **(a, e)** $t=400\ \mu\text{m}$ and $d=33\ \mu\text{m}$, **(b, f)** $t=400\ \mu\text{m}$ and $d=60\ \mu\text{m}$, **(c, g)** $t=400\ \mu\text{m}$ and $d=100\ \mu\text{m}$ and **(d, h)** $t=100\ \mu\text{m}$ and $d=35\ \mu\text{m}$

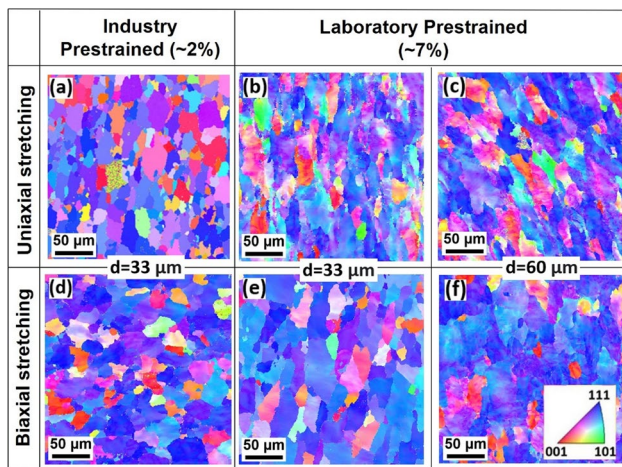
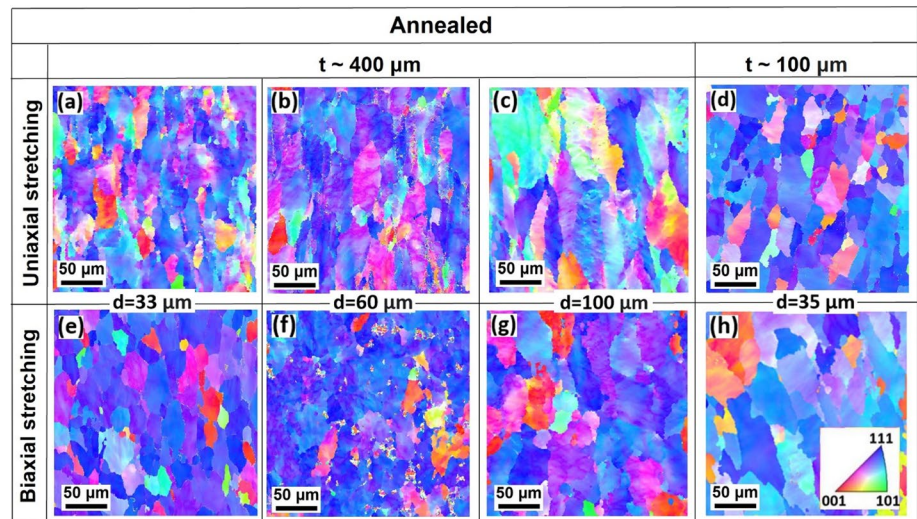


Fig. 7 Coloured inverse pole figure (IPF) maps of three different prestrained samples of about $400\ \mu\text{m}$ thickness after microforming under **a–c** uniaxial stretching and **d–f** biaxial stretching. Here, **(a, d)** industry prestrained to 2% with $d=33\ \mu\text{m}$, **(b, e)** laboratory prestrained to 7% with $d=33\ \mu\text{m}$, **(c, f)** laboratory prestrained to 7% with $d=60\ \mu\text{m}$

$k_{HP} \sim 482\ \text{MPa}\ \mu\text{m}^{-1/2}$. These values are in reasonable agreement with those reported for iron and low carbon steels. For example, Takaki et al. [22] established the following Hall–Petch equation for steels for the grain size region down to $0.2\ \mu\text{m}$:

$$\sigma_y(\text{MPa}) = 100 + 600d^{-1/2} \left(\mu\text{m}^{-1/2} \right)$$

Takeda et al. [23] studied the effects of C and N interstitials on the k_{HP} of Fe and reported that the k_{HP} increases with C content and gets saturated around $600\ \text{MPa}\ \mu\text{m}^{-1/2}$ when the carbon percentage exceeds 0.06%. The observed rise in σ_0 and decrease in k_{HP} values in ULC steels upon prestraining are consistent with the reported trend in the

literature. For example, the Hall–Petch plot shown in updated Fig. 8a also presents the results of Yang et al. [24] on ULC steels in both annealed and temper-rolled (skin-pass) to $\sim 2\%$ thickness reduction conditions. The increase in friction stress value in the prestrained ULC steel samples is not unexpected, as there will be a significant increase in the dislocation density within grains after prestraining to 7% leading to an increased barrier for further dislocation movement. The decrease in k_{HP} in prestraining samples can also be expected, as the stress required for propagating slip in adjacent grains across grain boundaries is lowered due to the back stress developed during prestraining.

4.3 Strain Hardening Behaviour

Figure 8b presents the strain hardening behaviour of four selected foils in terms of strain hardening rate, θ ($= d\sigma/d\epsilon$) versus the stress increment ($\sigma - \sigma_y$) obtained from the true stress-true strain curves. These samples were selected in order to address the effects of both the t/d ratio and the processing conditions. The $400\ \mu\text{m}$ thick annealed and prestrained foils exhibited stage-III (drastic fall in θ with stress increment) hardening and stage-IV (gradual drop in θ with stress increment). This represents the ideal work hardening behaviour of polycrystalline material. The prestrained foil showed a lesser extent of stage-III and stage-IV than its annealed counterpart. The slope of stage III hardening, k_{III} of the prestrained foil showed a mild difference compared to the $400\ \mu\text{m}$ thick annealed foil, whereas in an earlier work on similar material (under close prestrain values) the difference observed was considerably greater [13]. This might be due to the t/d effect, and the aforementioned study focussed on much thicker foils (sheets) with almost polycrystalline behaviour. The possible phenomenon behind this could be the increased presence of dislocation tangle-imposed

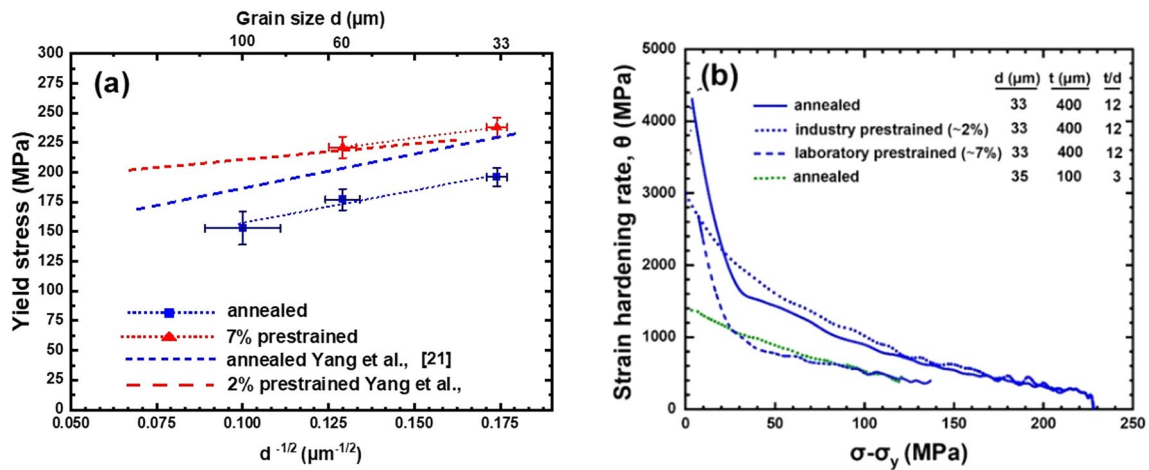
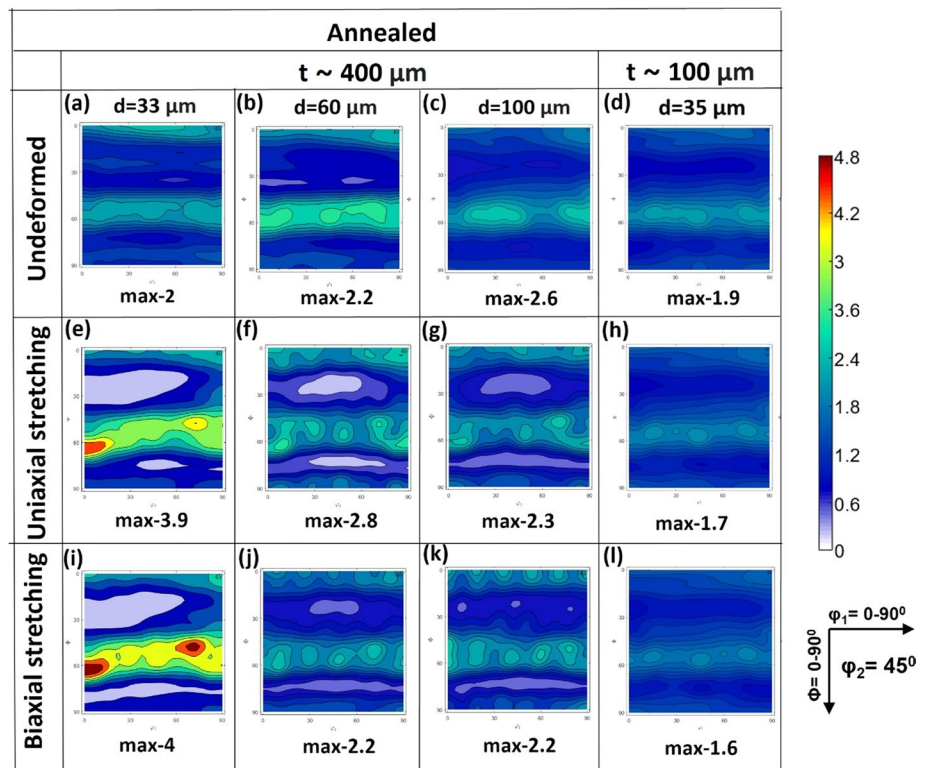


Fig. 8 **a** Hall–Petch plot in terms of the yield stress, σ_y versus (grain size) $^{-1/2}$, $d^{-1/2}$ of the annealed and prestrained ULC foils compared with the established relationships available for ULC steel in litera-

ture, and **b** strain hardening rate, θ versus the stress increment, $(\sigma - \sigma_y)$ plot calculated from the data of tensile curves shown in Fig. 4 for the selected annealed and prestrained foils

Fig. 9 Orientation distribution function (ODF) contour sections with constant $\phi_2 = 45^\circ$ for four different annealed samples in **a–d** undeformed state and after microforming under **e–h** uniaxial stretching and **i–l** biaxial stretching. Here, (**a**, **e**, **i**) $t = 400 \mu\text{m}$ and $d = 33 \mu\text{m}$, (**b**, **f**, **j**) $t = 400 \mu\text{m}$ and $d = 60 \mu\text{m}$, (**c**, **g**, **k**) $t = 400 \mu\text{m}$ and $d = 100 \mu\text{m}$ and (**d**, **h**, **l**) $t = 100 \mu\text{m}$ and $d = 35 \mu\text{m}$



barriers in prestrained foils, which led to reduced dislocation motion [25]. The annealed 100 μm thick foil with $t/d \sim 3$ and $d \sim 35 \mu\text{m}$ showed lesser values of θ than 400 μm thick foil, despite having the similar grain size, and also displayed a very negligible stage III hardening. This could be possibly due to higher free-surface annihilation intragranular dislocations than that of grain boundary (GB) dislocations (i.e., in a surface intragranular dislocations outnumber the GB dislocations) which is very likely in case of foils of with low

t/d ratios and thicknesses $\sim 100 \mu\text{m}$ [26]. Subsequently, the strain localization of softer grain interior regions occurs and thereby hinders further plastic deformation. Therefore, as a result of a lower thickness and a low t/d value, the increased Frank-Read (FR) type dislocations causing annihilation at free surfaces can lead to a considerable reduction in strength, strain hardening rate and consequently ductility [27–29]. Also, due to the free surface annihilation of dislocations,

the formation of dislocation tangles is very restricted in thin foils, hence the limited stage III hardening in thin foils [30].

4.4 Microformability and Texture Evolution

The Formability of a material is expected to vary with the grain size and thickness of the sheet, especially in foils due to contribution of surface grains to overall ductility and, in particular, strain hardening [30]. The observed lower limit strains with increasing grain size and decreasing thickness of foil (i.e., lower t/d ratios) can also be attributed to the premature microvoid coalescence, thereby leading to early microcrack growth through the foil thickness. This can be seen in the reduced non-uniform strains under the tensile loading path, which was the case in tensile stress–strain curves of the ULC steel foils with lower t/d ratios (Fig. 4 and Table 1). The observations of lower or at least equal forming strains under biaxial stretching when compared with a plane strain path in a low t/d ratio ULC steel foils are consistent with the reports of Peng et al. [31] on Cu foils, Meng et al. on SS304 foils [32] and our recent study on Cu foils [17]. Multiple factors, that have significant influence on scaling, such as friction, sheet/foil anisotropy [33], changes in fracture pattern at the microscale [33] etc., can affect the microformability of the metallic foils.

The limiting strains cannot be thoroughly correlated with the texture data. One main reason that the variation in the intensity of γ -(ND) $\langle 111 \rangle$ fiber in the initial condition of all the foils studied is minimal, which is an influential factor for limiting strain from a theoretical crystallographic texture point of view [34]. Nonetheless, there are differences in the evolution trends in different conditions, which can be discussed.

The texture evolution results were presented in Figs. 6, 7 and Figs. 9, 10 as IPFs and ODFs, respectively. In low carbon steels, deformation and annealing textures are usually presented in terms of γ -fiber (ND) $\langle 111 \rangle$ and θ -fiber (ND) $\langle 001 \rangle$. In the initial (annealed) condition prior to deformation (refer to Fig. 2), the foils exhibit the predominant presence of γ fibre component and a negligible presence of the $\alpha \langle 112 \rangle$ component. The annealing texture and the intensity of the γ fibre component, depends on grain size after hot rolling, carbon content, and factors such as the amount of cold reduction. It has been well-documented that, owing to their higher stored energies, the heavily cold-deformed grains with an (111) orientation have profoundly higher tendency to recrystallize than those grains of the other orientations in low carbon steels [1]. This preferred nucleation can lead to development of strong $\langle 111 \rangle$ ND γ -fiber recrystallized texture during annealing. This could be the reason for the presence of strong γ -fiber texture in the as-received 400 μm thick foils which were cold rolled plus batch annealed followed by skin-pass of 2% cold reduction.

It is to be noted that the as-received foils were then subsequently annealed at elevated temperatures to obtain a range of grain sizes by merely inducing grain growth. It has been reported that in low carbon steels there should be strengthening rather than weakening of the initial $\{111\}$ texture components during grain growth [35]. This clearly suggests that the formation of the θ -fiber component (presence of $\langle 001 \rangle$ orientation grains) apart from the retention of the prior γ -fiber texture in the laboratory annealed samples might be related to prior skin-pass reduction. An increase in the intensity of the γ -fiber can be found for the samples with coarser grains, possibly due to the nucleation of more $\gamma \langle 111 \rangle$ grains with the increased annealing time.

Under uniaxial and biaxial deformation modes, the initial $\gamma \langle 111 \rangle$ ND fiber was strengthened. By and large, the intensification of texture evolution under biaxial and uniaxial modes, is higher for samples with a higher t/d ratio of 12 (Fig. 9 e, i). In most cases pertaining to both annealed and prestrained foils, under both uniaxial and biaxial stretching modes, the strengthening of $\{111\} \langle 110 \rangle$ components of γ -fiber was more apparent than that of the $\{111\} \langle 112 \rangle$ components. A similar trend of evolution of the $\gamma \langle 111 \rangle$ ND fiber under uniaxial and biaxial deformation modes has also been reported elsewhere for the same material [3].

The phenomenon behind the higher intensification of $\gamma \langle 111 \rangle$ ND fiber texture under biaxial and uniaxial modes for the foils with the higher $t/d \sim 12$ accords to the postulation by Meyers and Chawla [36] which mentions a critical aspect of texture formation with the increase in degree of polycrystallinity. During the deformation of the specimen with $t/d \sim 12$, slip of grains in their appropriate glide systems and grain rotation (with a higher level of constraint from neighbouring grains than lower t/d ratio specimens) are the two probable mechanisms. This results in the development of a strong preferred orientation under large strains due to the likely alignment of preferred slip directions with the direction of deformation. The increased intensity of texture components under biaxial stretching as compared to that under uniaxial stretching is not an unexpected result, as foils/sheets experience an increased effective strain in the former strain path than in the later strain path.

5 Conclusions

The following key conclusions can be drawn from the present study on the effects of the grain size, thickness of foil i.e., t/d ratio and the state of material (annealed vs. prestrained) on deformation and texture evolution in ULC steel foils:

1. Upon annealing the starting foil in cold rolled plus annealed and skin pass rolled to ~2%, the ULC steel foil developed slight θ -fiber ($\langle 001 \rangle \parallel \text{ND}$) component along with retention of most of the initial typical strong γ -fiber ($\langle 111 \rangle \parallel \text{ND}$) texture. Furthermore, there were no noticeable changes in microstructure and texture of the samples upon further prestraining to 7%.
2. All the annealed samples showed a typical yield-point phenomenon; however, the total yield-point elongation increased while non-uniform strain decreased with decreasing the t/d ratio. Both the strength and ductility reduced drastically in the 100 μm thin foil against the 400 μm thick foil for a similar grain size. At a higher percentage of prestraining (~7%), the ductility significantly dropped while there was an increase in yield strength due to prior cold working. In summary, with decreasing the t/d ratio there was a pronounced drop in both strength, ductility and strain hardening rate due to the increased share of surface grains.
3. Both the annealed and prestrained samples showed typical Hall–Petch strengthening i.e., an increased yield stress with decreasing the grain size; however, the Hall–Petch coefficient (k_{HP}) value decreased while the friction stress value of ULC steel increased upon prestraining.
4. All foils showed typical forming limit curves, but with slight lowering in major strain values in the biaxial strain path than typically seen in sheet forming. Moreover, the overall limiting strain values decreased with decreasing the t/d ratio and increasing the prestrain level as well.
5. The texture evolution study highlights the strengthening of γ -fiber ($\langle 111 \rangle \parallel \text{ND}$), especially $\{111\} \langle 110 \rangle$ components with intensities more sensitive to t/d ratio of the foils than the strain path variation.

Acknowledgements The authors are grateful to M/s Theis Precision Steel India Private Limited for providing us ULC steel sheets and foils for the present study. The authors would like to thank the OIM-Texture lab, IIT Bombay for giving access to the EBSD and XRD texture facilities. The authors acknowledge the FIST-UTM (Mechanical characterization) lab for providing the UTM for conducting the tensile and forming experiments. The authors are thankful to Prof. Pradeep Dixit, Department of Mechanical Engineering, IIT Bombay for facilitating to use the Olympus DSX100 opto-digital microscope.

Funding No funding is received for the present study.

Declarations

Conflict of interest The authors have no competing interests to declare that are relevant to the content of this article.

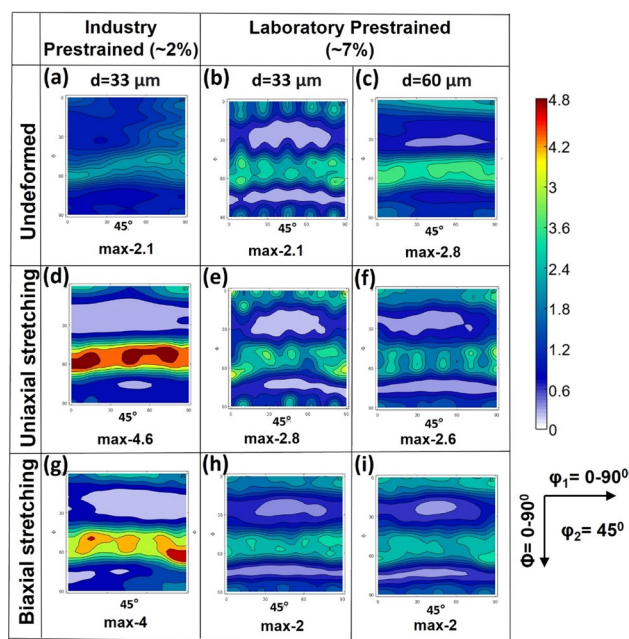


Fig. 10 ODF contour sections with constant $\phi_2 = 45^\circ$ of four different prestrained samples in **a–c** undeformed state and after microforming under **d–f** uniaxial stretching and **g–i** biaxial stretching. Here, **(a, d, g)** industry prestrained to 2% with $d = 33 \mu\text{m}$, **(b, e, h)** laboratory prestrained to 7% with $d = 33 \mu\text{m}$, **(c, f, i)** laboratory prestrained to 7% with $d = 60 \mu\text{m}$

References

1. D.T. Llewellyn, R.C. Hudd, *Steels: Metallurgy and Applications* (Butterworth-Heinemann, Oxford, 1998)
2. C. Capdevila, C. Garcia-Mateo, F.G. Caballero, C. Garcia de Andres, Neural network analysis of the influence of processing on strength and ductility of automotive low carbon sheet steels. *Comp. Mater. Sci.* **38**, 192–201 (2006). <https://doi.org/10.1016/j.commater.2006.02.005>
3. P. Antoine, S. Vandeputte, J.B. Vogt, Effect of microstructure on strain-hardening behaviour of a Ti-IF steel grade. *ISIJ Int.* **45**, 399–404 (2005). <https://doi.org/10.2355/isijinternational.45.399>
4. P. Antoine, S. Vandeputte, J.B. Vogt, Empirical model predicting the value of the strain-hardening exponent of a Ti-IF steel grade. *Mater. Sci. Eng. A* **433**, 55–63 (2006). <https://doi.org/10.1016/j.msea.2006.06.030>
5. C. Capdevila, J.P. Ferrer, F.G. Caballero, C. Garcia de Andres, Influence of processing parameters on the recrystallized microstructure of extra-low-carbon steels. *Metall. Mater. Trans. A* **37**, 2059–2068 (2006). <https://doi.org/10.1007/bf02586126>
6. G.E. Dieter, D. Bacon, *Mechanical Metallurgy* (McGraw-Hill, New York, 1976)
7. W.F. Hosford, *Mechanical Behavior of Materials* (Cambridge University Press, Cambridge, 2010). <https://doi.org/10.1017/s0001924000088126>
8. G. Simons, Ch. Weippert, J. Dual, J. Villain, Size effects in tensile testing of thin cold rolled and annealed Cu foils. *Mater. Sci. Eng. A* **416**, 290–299 (2006). <https://doi.org/10.1016/j.msea.2005.10.060>
9. M. Klein, A. Hadrboletz, B. Weiss, G. Khatibi, The ‘size effect’ on the stress–strain, fatigue and fracture properties of thin metallic

- foils. *Mater. Sci. Eng. A* **319**, 924–928 (2001). [https://doi.org/10.1016/s0921-5093\(01\)01043-7](https://doi.org/10.1016/s0921-5093(01)01043-7)
10. J. Kim, R. Golle, H. Hoffmann, Investigation of size effects of very thin aluminum and copper sheets using aero-bulge test. *Mater. Sci. Eng. A* **527**, 7220–7224 (2010). <https://doi.org/10.1016/j.msea.2010.07.076>
 11. M.W. Fu, W.L. Chan, A review on the state-of-the-art microforming technologies. *Int. J. Adv. Manuf. Technol.* **67**, 2411–2437 (2013). <https://doi.org/10.1007/s00170-012-4661-7>
 12. J. Sahu, S. Chakrabarty, R. Raghavan, S. Mishra, Investigations of size effect on formability and microstructure evolution in SS304 thin foils. *J. Strain Anal.* **53**(7), 517–528 (2018). <https://doi.org/10.1177/0309324718792443>
 13. E. Hoggan, R. Scott, M.R. Barnett, P.D. Hodgson, Mechanical properties of tension levelled and skin passed steels. *J. Mater. Proc. Technol.* **125**, 155–163 (2002). [https://doi.org/10.1016/s0924-0136\(02\)00368-0](https://doi.org/10.1016/s0924-0136(02)00368-0)
 14. C.H. Chen, R.S. Lee, J.T. Gau, Size effect and forming-limit strain prediction for microscale sheet metal forming of stainless steel 304. *J. Strain Anal. Eng. Design* **45**, 283–299 (2010). <https://doi.org/10.1243/03093247jsa585>
 15. J.S.H. Lake, Control of discontinuous yielding by temper rolling. *J. Mech. Work. Technol.* **12**, 35–66 (1985). [https://doi.org/10.1016/0378-3804\(85\)90041-5](https://doi.org/10.1016/0378-3804(85)90041-5)
 16. J.-R. Kim, A. Eun-Yeong, H. Das, J. Yong-Ha, H. Sung-Tae, M. Miles, L. Kwang-Jin, Effect of tool geometry and process parameters on mechanical properties of friction stir spot welded dissimilar aluminum alloys. *Int. J. Prec. Eng. Manuf.* **18**, 445–452 (2017). <https://doi.org/10.1007/s12541-017-0053-0>
 17. J.S. Ibrahim, R.T. Mathew, M.J.N.V. Prasad, K. Narasimhan, Processing and specimen thickness to grain size (t/d) ratio effects on tensile behaviour and microformability of copper foils. *Met. Mater. Int.* **28**, 2340–2355 (2022). <https://doi.org/10.1007/s12540-021-01145-w>
 18. R. Abbaschian, L. Abbaschian, R.E. Reed-Hill, *Physical Metallurgy Principles*, 4th edn. (Cengage Learning, USA, 2009)
 19. W.G. Johnston, J.J. Gilman, Dislocation velocities, dislocation densities, and plastic flow in lithium fluoride crystals. *J. App. Phys.* **30**, 129–144 (1959). <https://doi.org/10.1063/1.1735121>
 20. E.O. Hall, The deformation and ageing of mild steel: III discussion of results. *Proc. Phys. Soc. Sect. B* **64**, 747 (1951). <https://doi.org/10.1088/0370-1301/64/9/303>
 21. N.J. Petch, The cleavage strength of polycrystals. *J. Iron Steel Inst.* **174**, 25–28 (1953)
 22. S. Takaki, K. Kawasaki, Y. Kimura, Mechanical properties of ultra-fine grained steels. *J. Mater. Proc. Technol.* **117**, 359–363 (2001). [https://doi.org/10.1016/s0924-0136\(01\)00797-x](https://doi.org/10.1016/s0924-0136(01)00797-x)
 23. K. Takeda, N. Nakada, T. Tsuchiyama, S. Takaki, Effect of interstitial elements on Hall–Petch coefficient of ferritic iron. *ISIJ Int.* **48**, 1122–1125 (2008). <https://doi.org/10.2355/isijinternational.48.1122>
 24. L.L. Yang, T. Nakagaito, Y. Funakawa, K. Kojima, change in yield strength of Nb-bearing ultra-low carbon steels by temper-rolling. *Mater. Sci. Forum* **941**, 230–235 (2018). <https://doi.org/10.4028/www.scientific.net/msf.941.230>
 25. A.D. Rollett, U.F. Kocks, A review of the stages of work hardening. *Solid State Phen.* **35-36**, 1–18 (1993). <https://doi.org/10.4028/www.scientific.net/ssp.35-36.1>
 26. Y. Akiniwa, T. Suzuki, K. Tanaka, Evaluation of deformation behavior in Cu thin film under tensile and fatigue loading by X-ray method. *Mater. Sci. Forum* **524**, 807–812 (2006). <https://doi.org/10.4028/www.scientific.net/msf.524-525.807>
 27. C. Shen, Z. Zhu, D. Zhu, J. Ren, Copper deposits with high tensile strength and elongation electroformed in an ultra-low-concentration sulfate bath without additives. *J Mater Eng Perf* **26**, 987–992 (2017). <https://doi.org/10.1007/s11665-016-2494-5>
 28. S. Fujiwara, K. Abiko, Ductility of ultra high purity copper. *Le J. de Phys. IV* **5**, C7-295 (1995). <https://doi.org/10.1051/jp4:1995735>
 29. M. Shakeri, A. Sadough, B.M. Dariani, Effect of pre-straining and grain size on the limit strains in sheet metal forming. *Proc. Inst. Mech. Eng. Part B: J. Eng. Manuf.* **214**, 821–827 (2000). <https://doi.org/10.1243/0954405001517892>
 30. W.L. Chan, M.F. Fu, J. Lu, J.G. Liu, Modeling of grain size effect on micro deformation behavior in micro-forming of pure copper. *Mater. Sci. Eng. A* **527**, 6638–6648 (2010). <https://doi.org/10.1016/j.msea.2010.07.009>
 31. L.F. Peng, Z.T. Xu, M.F. Fu, X.M. Lai, Forming limit of sheet metals in meso-scale plastic forming by using different failure criteria. *Int. J. Mech. Sci.* **120**, 190–203 (2017). <https://doi.org/10.1016/j.ijmecsci.2016.11.021>
 32. B. Meng, Y.Y. Zhang, C. Cheng, J.Q. Han, M. Wan, Effect of plastic anisotropy on microscale ductile fracture and microformability of stainless steel foil. *Int. J. Mech. Sci.* **148**, 620–635 (2018). <https://doi.org/10.1016/j.ijmecsci.2018.09.027>
 33. P. Van Houtte, L. Delannay, I. Samajdar, Quantitative prediction of cold rolling textures in low-carbon steel by means of the LAMEL model. *Text. Stress Microstruct.* **31**, 109–149 (1999). <https://doi.org/10.1155/2008/173083>
 34. I. Samajdar, B. Verlinden, P. Van Houtte, Developments in macro and micro texture during plane strain channel die compression of IF steel. *ISIJ Int.* **38**, 759–765 (1998). <https://doi.org/10.2355/isijinternational.38.759>
 35. S.K. Yerra, H.V. Vankudre, P.P. Date, I. Samajdar, Effect of strain path and the magnitude of prestrain on the formability of a low carbon steel: on the textural and microtextural developments. *J. Eng. Mater. Technol.* **126**, 53–61 (2004). <https://doi.org/10.1007/s10749-019-01047-3>
 36. M.A. Meyers, K.K. Chawla, *Mechanical Behavior of Materials* (Cambridge University Press, Cambridge, 2008). <https://doi.org/10.1017/cbo9780511810947>

Publisher's Note Springer Nature remains neutral with regard to jurisdictional claims in published maps and institutional affiliations.

Springer Nature or its licensor (e.g. a society or other partner) holds exclusive rights to this article under a publishing agreement with the author(s) or other rightsholder(s); author self-archiving of the accepted manuscript version of this article is solely governed by the terms of such publishing agreement and applicable law.